Design and test of a positive-negative pressure quinoa precision seed-metering device with a disturbed seed-filling mechanism

Xiaoshun Zhao[1], Zhuangzhuang Hou[1], Wei Lyu[2*], Chuan Lu[2], Huali Yu[1], Zhimin Wei[3]

(1. *College of Mechanical and Electrical Engineering, Hebei Agricultural University, Baoding 071001, China*;
2. *The Science and Technology Innovation Service Center of Hebei Province, Shijiazhuang 050035, China*;
3. *Institute of Millet Crops, Hebei Academy of Agriculture and Forestry Sciences, Shijiazhuang 050035, China*)

Abstract: Aiming at the problem of difficulties in seed filling and seed cleaning caused by the small specific gravity, small size, and irregularity of quinoa seeds, a positive-negative pressure precision seed-metering device for quinoa seeds with a disturbed seed-filling mechanism was designed. The disturbed seed-filling mechanism can improve the seed-filling performance of the precision seed-metering device and reduce the power consumption required by the forced-draught fan. Positive pressure seed cleaning can solve the problem of pore blockage caused by small and light quinoa seeds and improve work stability. Taking Jili No. 3 seed as the research object, simulation analysis of the flow field in the air chamber of the precision seed-metering device was carried out by the Fluent 2021 R1 software. The influence of seed-sucking hole structure parameters (shape and number of seed-sucking holes, inclination angle of seed-sucking holes, and diameter of seed-sucking holes) on the flow field was analyzed by a pressure nephogram and a velocity vectogram. The optimal parameter combination was obtained as follows: a circular-cone-type shape of the seed-sucking hole, a number of 20 seed-sucking holes, a 70° inclination angle of the seed-sucking hole, and a 1 mm diameter of the seed-sucking hole. EDEM 2020 software and orthogonal test were used to optimize the design of the disturbed seed-filling mechanism. The influence of structural parameters of the disturbed seed-filling mechanism (groove radius of the disturbed seed-filling mechanism (GRDSM), arc of the disturbed seed-filling mechanism (ADSM), and position angle of the disturbed seed-filling mechanism (PADSM)) on the qualified index (I_q) of scooping seeds was analyzed. The optimal parameter combination was obtained: 1.3 mm GRDSM, 140° ADSM, and 25° PADSM. With the help of the JPS-12 test-bench, a response surface test was carried out with the qualified index (I_q), the miss index (I_{miss}), and the multiple index (I_{mul}) as test indices, and the seed-sucking negative pressure, the seed-metering device rotation speed, and the seed-falling height as test factors. The optimal working parameter combination was obtained: –3.0 kPa seed-sucking negative pressure, 15 r/min seed-metering device rotation speed, 100 mm seed-falling height. Validation tests were carried out on the optimized seed-metering device, and the results showed that the I_q was 82.5%, the I_{miss} was 6.5%, and the I_{mul} was 11%, which met the index requirements in JB/T 10293-2013 Technical conditions of single seed (precision) seeder. The results of this study can provide a reference for the design of machinery for the precision seeding of small seeds such as quinoa.

Keywords: quinoa, precision seed-metering device, disturbed seed-filling mechanism, positive-negative pressure, Fluent, EDEM, response surface test

DOI: 10.25165/j.ijabe.20241706.9211

Citation: Zhao X S, Hou Z Z, Lyu W, Lu C, Yu H L, Wei Z M. Design and test of a positive-negative pressure quinoa precision seed-metering device with a disturbed seed-filling mechanism. Int J Agric & Biol Eng, 2024; 17(6): 121–134.

1 Introduction

Quinoa is a small-grained crop whose characteristics, such as small specific gravity, irregular shape, and poor fluidity, place high demands on the seed-metering device. Therefore, there have been serious shortcomings in the mechanized planting of quinoa for a long time, which restrict the large-scale production and industrialization of quinoa. Given this situation, the research on the quinoa precision seed-metering device can not only improve the planting quality of quinoa, especially the efficiency of seed filling and seed cleaning in the seeding process, but also reduce the planting difficulty of quinoa and other small-grain crops. The common methods of quinoa seeding are mainly strip cropping and bunch planting. The seeding machinery of strip cropping mostly adopts a tooth wheel-type seed-metering device, and the seeding machinery of bunch planting mostly adopts a duckbill-type laminating bunch-planting seed-metering device. Although this kind of mechanical seed-metering device has good adaptability to seeds, it has a high seed injury rate, low seeding efficiency, and cannot achieve precision seeding[1,2].

In recent years, scholars at home and abroad have shifted the research focus of the small-size seed precision seed-metering device to the negative pressure type. The negative pressure-type precision seed-metering device has better adaptability to the shape and size of the seeds, does not easily damage the seeds, and provides a better

Received date: 2024-07-09 **Accepted date:** 2024-11-10

Biographies: **Xiaoshun Zhao**, PhD, Associate Professor, research interest: modern agricultural equipment design and control, precision planting, Email: zhao_xsh@126.com; **Zhuangzhuang Hou**, MS candidate, research interest: agricultural mechanization, Email: hzz6666662023@163.com; **Chuan Lu**, Master, Assistant Researcher, research interest: crop breeding, Email: luchuan0602@126.com; **Huali Yu**, MS, Associate Professor, research interest: vehicle engineering, Email: 48796619@qq.com; **Zhimin Wei**, MS, Associate Researcher, research interest: crop breeding, Email: weizhimincn@126.com.

***Corresponding author: Wei Lyu**, BS, Associate Researcher, research interest: crop breeding. The Science and Technology Innovation Service Center of Hebei Province, Shijiazhuang, 050035, Hebei, China. Tel: +86-13930125879, Email: lvwei91@126.com.

choice for precision seeding of small-sized crops. Zhang et al.[3,4] used bench tests, DEM and CFD simulation technology to obtain the optimal structural parameter range of the small particle size air-suction-type seed-metering device. Wang et al.[5] developed a forked seed sorter based on the air-suction-type seed-metering device that could realize precision seeding operations with narrow row spacing. Based on the principles of negative pressure seed extraction and broken pressure seeding, Zeng et al. developed an air-suction bunch planting-type pepper precision seed-metering device[6]. Zhao designed a positive-negative pressure wide seedling belt-type wheat precision seed-metering device. The structural parameters of the seed-sucking holes and the range of working parameters of the seed-metering device were determined by Fluent software and the EDEM-Fluent coupling technology at that time, and the optimal combination of parameters was obtained by a stepping pedestal test[7]. Liao et al. developed a positive-negative pressure tubular needle-type collecting and metering device of western ginseng, and constructed a mechanical model of the seed-metering device during seed sucking and seed falling[8]. Abdolahzare et al. explored the effects of vacuum negative pressure and the rotation speed of the planter plate on the working performance of the seed-metering device[9]. Singh et al. explored the effects of the seed-metering device rotation speed, the seed-sucking negative pressure, and the seed-sucking hole structure parameters on the performance of the seed-metering device[10]. It can be seen from the above that the current research on the small particle size crop seed-metering device is mainly focused on negative pressure types, and it is still in the stage of continuous research and improvement. Due to the small specific gravity and small size of small-grained crops such as quinoa, a negative pressure-type seed-metering device makes it difficult to clean seeds by their weight[11]. Although the positive-negative pressure-type seed-metering device is conducive to the seed-cleaning of small-grained seeds, it is not conducive to the seed-filling of small-grained seeds with irregular shapes[12].

In this paper, a positive-negative pressure quinoa precision seed-metering device with a disturbed seed-filling mechanism is designed. Compared with the traditional negative pressure-type seed-metering device, it can improve the seed-filling performance, seed-cleaning efficiency, and working stability of the seed-metering device, and it is suitable for irregular small-size seeds such as quinoa. At the same time, it reduces the power consumption of the forced-draught fan during the working process of the seed-metering device.

2 Materials and methods

2.1 Analysis of seed-metering device structure and parameters

2.1.1 Three-dimensional dimensions of quinoa

The three-dimensional size of the quinoa seed is an important basis for the design of the structural parameters of the seed-metering device. To determine the structural parameters of the seed-metering device in the follow-up study, taking Jili No. 3 seed as the object of study, 100 seeds were randomly selected to measure the dimensions of the three directions of seed length, seed breadth, and seed thickness. The selection of measurement locations in each direction is shown in Figure 1, and the measurement results are shown in Table 1.

After the measurement process, the length range of the quinoa seeds is found to be 1.91-2.35 mm, the width range is 1.81-2.28 mm, and the thickness range is 0.98-1.28 mm. The size is basically in line with the normal distribution. As can be seen from Table 1, the average length of the quinoa seeds is 2.16 mm, the average width is 2.04 mm, and the average thickness is 1.16 mm. Considering that the difference in length and width of the quinoa seeds is small, the quinoa seed is simplified into a disc shape, which is convenient for the design and parameter determination of the key structure of the seed arranger in the later stage.

a. Seed length b. Seed width c. Seed thickness

Figure 1 Seed triaxial dimension diagram

Table 1 Three-dimensional size of quinoa seeds

Parameters	Average/mm	Standard deviation/mm	Variation coefficient/%
Length	2.16	0.22	10.2
Width	2.04	0.23	11.3
Thickness	1.16	0.15	12.9

2.1.2 Structure and working principle of seed-metering device

The positive-negative pressure quinoa precision seed-metering device with a disturbed seed-filling mechanism is mainly composed of an air chamber, a seed tray, a disturbed seed-filling mechanism, a seed box, a transmission gear, a drive shaft, a sealing ring, and a bearing. The structure explosion diagram is shown in Figure 2.

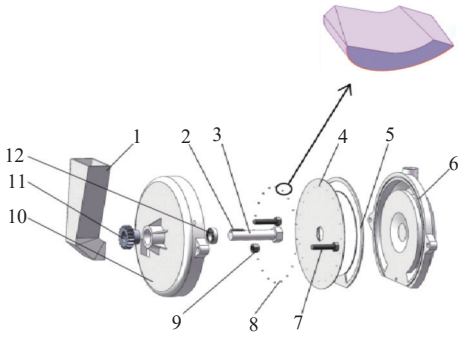

1. Seed box 2. Key 3. Drive shaft 4. Planter plate 5. Sealing ring 6. Air chamber 7. Bolt 8. Disturbed seed-filling mechanism 9. Nut 10. Seed-filling room 11. Transmission gear 12. Bearing

Figure 2 Structure explosion diagram of the precision seed-metering device

The working principle of the seed-metering device is shown in Figure 3. The disturbed seed-filling mechanism first scoops up the seeds in the seed-scooping area, and then the scooped seeds follow the movement of the disturbed seed-filling mechanism to the seed-sucking area. Under the action of negative pressure suction, the seeds are adsorbed on the planter plate, and follow the planter plate smoothly through the seed-carrying area into the seed-falling area. In the seed-falling area, the negative pressure suction disappears, and the seeds break away from the planter plate under the action of their gravity and complete the seed fall. The seeds that do not fall in time follow the planter plate into the seed-cleaning area under the action of positive pressure, and detach from the planter plate blowing force to complete the seed cleaning. The negative pressure area of the seed-metering device is a ring structure, which ensures the uniformity of the flow field distribution in the negative pressure air chamber[13]. Under the action of the forced-draught fan, the external airflow of the planter plate flows into the negative pressure air chamber through the molded hole to form an airflow channel. The channels create a pressure difference between the two sides of

the planter plate and adsorb the seeds into the seed-sucking holes. The disturbed seed-filling mechanism is stuck on the planter plate to provide a certain support force to the seeds, so as to counteract the friction force on the seed-sucking holes and the squeezing force of the surrounding seeds on it during seed filling. One side of the drive shaft is equipped with a sprocket, and the power transmission is completed through the chain to realize the rotation of the planter plate.

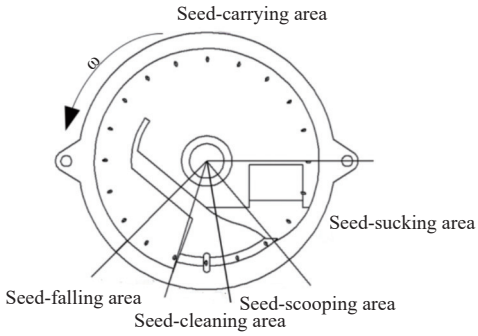

Figure 3 Working principle diagram of the seed-metering device

Referring to the specific stress of the small-size crops in each area of the seed-metering device [14], compared with the two cases with or without a disturbed seed-filling mechanism, the negative pressure vacuum required to carry the seeds in the planter plate is smaller when the quinoa seeds are in the seed-filling area and the seed-carrying area. Therefore, in the case of the disturbed seed-filling mechanism, the required forced-draught fan power consumption is lower, and quinoa seeds are more likely to fall off in the seed-filling area due to the effect of positive pressure blowing.

2.1.3 Key structural parameters of the seed-metering device

As an important part of the seed-metering device, the planter plate has a significant impact on its effect. The design of the planter plate mainly includes two parts: one is the design of structural parameters, including the diameter of the planter plate and the shape, size, and number of seed-sucking holes, and the other is the determination of the speed range of the planter plate.

The filling time of the seed-metering device is an important parameter to determine the seed filling performance. The relationship between the seed filling time and the parameters of the planter plate is as follows[7]:

$$\begin{cases} T = \dfrac{L_r}{v_1} \\ L_r = \alpha\left(\dfrac{d_p}{2} - r_k\right) \\ v_1 = \omega\left(\dfrac{d_p}{2} - r_k\right) \\ \omega = \dfrac{\pi n_1}{30} \end{cases} \tag{1}$$

where, T is seed filling time, s; L_r is arc length of the seed-filling area, mm; v_1 is the line velocity at seed-sucking holes, m/s; α is seed-filling angle, rad; d_p is planter plate diameter, mm; r_k is the distance between the center of the seed-sucking hole and the edge of the planter plate, mm; ω is the planter plate angular velocity, rad/s; and n_1 is rotation speed of the planter plate, r/min.

It is obtained by organizing according to Equation (1):

$$T = \frac{30\alpha}{\pi n_1} \tag{2}$$

The diameter of the planter plate is one of the important parameters of the planter plate, which has a significant impact on the overall size of the seed-metering device, the number of seed-sucking holes, the speed of the seed-metering device, and the size of other parts. According to the "Agricultural Machinery Design Manual", in the range of the diameter of the planter plate (140-260 mm) and combined with the agronomic requirements of quinoa planting, the diameter of the planter plate is determined to be 220 mm. According to the shape of quinoa seeds, their adsorption posture on the seed-sucking hole is mainly in two ways: flat-lying type and side-standing type.

According to Table 1, combined with Equation (3) for the relationship between seed-sucking hole diameter and seed size in the "Agricultural Machinery Design Manual", the diameter parameters of the seed-sucking holes under different adsorption postures are 1.16-1.55 mm (flat-lying type) and 0.57-0.84 mm (side-standing type), respectively. Taking into account the size difference of quinoa seeds, the diameter range of the seed-sucking holes is preliminarily set to 0.6-1.6 mm. Since the diameter of the seed-sucking hole has a direct impact on the seed-sucking negative pressure, it is necessary to further adjust the range according to the seed-sucking negative pressure.

$$d = (0.64 \sim 0.66)b \tag{3}$$

where, b is the mean radius of the seed, mm.

The number of seed-sucking holes has a great influence on the filling performance[15]. The number of seed-sucking holes is generally calculated according to Equation (4) :

$$Z = \frac{\pi d_p v_2 (1+\zeta)}{v_1 L} \tag{4}$$

where, v_2 is the planter advance speed (m/s), ζ is the planter wheel slip rate (%).

According to the "Agricultural Machinery Design Manual", the slip rate of the ground wheel is 0.05-0.12, and the linear speed at the seed-sucking holes cannot be more than 0.35 m/s; otherwise, the working efficiency of the seeder will be greatly reduced. According to the agronomic requirements and related data[16-18], the grain spacing of quinoa is between 100 and 300 mm, and the working speed of the seeder is between 1.5 and 4.0 m/s. Substitution of the aforementioned parameters yields an estimated range for the number of seed-sucking holes, which is between 12 and 44.

The rotation speed of the planter plate has an important impact on the working performance of the seed-metering device. The formula for the relationship between the filling time and the rotation speed of the planter plate is as follows[18]:

$$n_1 = \frac{60 v_2}{ZL} \tag{5}$$

where, Z is the number of seed-sucking holes; and L is the theoretical grain spacing, m.

According to relevant references[19,20], r_k is generally taken as 15-20 mm, and the diameter of the seed-sucking hole distribution circle is generally 100-230 mm. Since the seed size of quinoa is relatively small, the r_k is taken as 15 mm, and the diameter of the distribution circle of the seed-sucking hole is taken as 190 mm. Combining Equation (1) and Equation (5) yields:

$$n_1 = \frac{30\omega}{\pi} \tag{6}$$

By bringing the parameters into Equation (6), the maximum value of the rotational speed of the planter plate is not more than 35 r/min.

By querying the "Agricultural Machinery Design Manual" and referring to the current domestic positive-negative pressure quinoa precision seed-metering device size, the final seed-sucking hole size

range is 0.8-1.6 mm. At the same time, when the size of the seed-sucking holes is too small, the maximum negative pressure required by the air chamber is larger. When the seed-sucking hole sizes are 0.8 mm and 1.6 mm, the corresponding negative pressure ranges of the air chamber are 0.26-3.14 kPa and 0.48-5.69 kPa, respectively. The range of negative pressure values in the air chamber is finally designed to be 0.26-5.7 kPa.

2.2 Model processing

SolidWorks 2017 software is utilized to establish a three-dimensional model of the seed-metering device with different structural parameters. According to the characteristics of the flow field distribution, the simulation model is divided into two main regions: a negative pressure-type air chamber and a seed-sucking hole. Before importing the model, the seed-sucking holes of the planter plate are numbered to facilitate subsequent analysis. The seed-metering device model is simplified and imported into Space Claim 2021 R1 for volume extraction and modeling of the flow field, which is shown in Figure 4.

a. Three-dimensional model of air chamber b. Cross-sectional view of the air chamber c. Air chamber fluid domain

Figure 4 Fluid domain model

Volume extraction is performed on the model. The established fluid domain is imported into the fluid domain model into the mesh module in Fluent 2021 R1, and the meshing method is a tetrahedral mesh. The curvature capture is utilized to encrypt the local mesh in the fluid domain, generating a 5-percent expansion layer near the wall. After overall mesh is generated, the mesh quality is checked and adjusted, and the orthogonal quality of more than 90% of the mesh is at 0.5 or above. The divided mesh is shown in Figure 5.

After the fluid domain is established, we select the names of each part in Space Claim 2021 R1. Since the simulation here is steady-state, there is no need to set up an interface, so only one fluid domain is required, which is named “fluid”. The negative pressure-type air intake is named the “inlet”, the side of the seed-sucking hole that touches the atmosphere is named the “outlet”, and the rest is named the “wall”.

2.3 Model processing

Before the boundary definition and condition setting, we need to judge the flow state of the fluid. In fluid mechanics, the Reynolds number is generally used to judge the flow state of the airflow[21], which is calculated by Equation (7).

$$Re = \frac{\rho v L}{\mu} \tag{7}$$

where, ρ is the fluid density, kg/m^3; v is the fluid velocity, m/s; L is the characteristic length of fluid, m; and μ is the dynamic viscosity, Pa·s.

The range of Reynolds numbers for laminar and turbulent flow is shown in Equation (8):

$$\begin{cases} Re < 2300, & \text{Laminar flow} \\ 2300 < Re < 4000, & \text{Transitional flow} \\ Re > 4000, & \text{Turbulence} \end{cases} \tag{8}$$

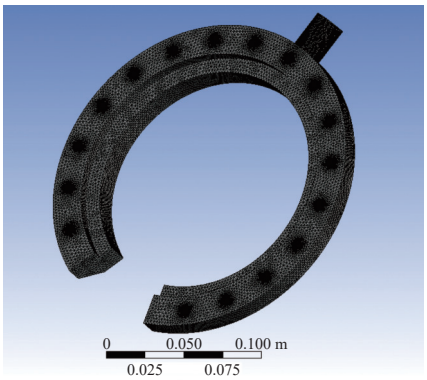

a. Grid after flow field division

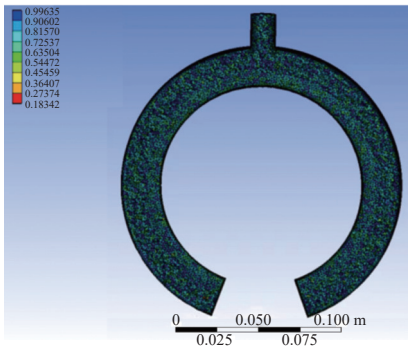

b. Flow field grid profile

Figure 5 Fluid domain model

At room temperature, the parameters of the air are obtained as follows: ρ is 1.21 kg/m^3, μ is 1.79×10^{-5} Pa·s, and L is 1×10^{-3} m. Due to the small aperture of the seed-sucking hole, the value of the fluid velocity should be appropriately increased to 70 m/s. Substituting the parameters into Equation (7) calculates the air as turbulent.

The solver and environment are set up using the governing equations based on the finite volume method. The solver is selected as the pressure solver for steady state solutions. The standard k-ε model is chosen for the turbulence model, and the wall function is chosen as standard. The fluid material is air, the solution is performed at a density of ρ = 1.21 kg/m^3, a reference atmospheric pressure of 101 325 Pa, and the other terms are kept at the default settings. The boundary definition and condition settings are set according to the settings in the pre-processing, the sides of the seed-sucking holes that touch the atmosphere (outlet 1-17) are designed as pressure outlets, and the pressure is set to 0 kPa. The end face of the pipe connected to the forced-draught fan is set to a pressure inlet, whose pressure is valued according to the negative vacuum pressure of the adsorbed seeds on the seed-sucking holes when the quinoa seeds move to the seed-carrying area. The pressure-velocity coupling method for solving the control parameters is SIMPLE, and the pressure interpolation method is selected as standard[21]. The residual convergence basis is set to 1×10^{-3} after initialization, and the fluid mass velocities at the inlet and outlet are monitored. After many iterations of computation, the overall iteration situation is balanced when iterating 620 steps. The mass of the fluid at all inlets and outlets are calculated by the Reports-Fluxes-mass flow rate in the Fluent module, and the poor quality is calculated to be less than 0.5%, which can be judged as convergence. Therefore, the number of iteration steps in the subsequent simulation is set to 700.

2.4 Pre-processing settings

The three-dimensional model of the seed-metering device is simplified, saved in STP format, and imported into EDEM. In order to keep the model from deforming during import, we select manual

mesh size and adjust the minimum size to 0.2 mm and the maximum angle to 10°. The EDEM analysis model is shown in Figure 6. Setting the various material parameters and contact parameters in EDEM, the contact model is set as the Hertz-Mindlin (no slip) model, the particle plant is set at the mouth of the seed box, the gravitational acceleration is set at 9.81 m/s^2, the direction is along the positive direction of the *Z*-axis, the initial falling speed of the particles is set at 2 m/s, and the direction is the same as the direction of gravity. According to the meaning of the Rayleigh time step, the time step is set to 19% of the Rayleigh time step (approximately 3×10^{-6} s). The save interval should be appropriately increased to 0.01 s.

Figure 6 EDEM analysis mode

The EDEM simulation is divided into two times: the first time is the seed-filling phase of quinoa seeds for 1 s, and the second time is the beginning of the rotation of the planter plate for 10 s. The simulation is performed for a total time of 11 s.

2.5 Monitoring point setup

In order to investigate the effect of different parameters of the disturbed seed-filling mechanism on the scooping performance, it is necessary to set up monitoring points in a reasonable manner. To complete the design of the seed-filling room and the disturbed seed-filling mechanism, a total of two monitoring points are required. The first monitoring point is used to monitor the number of quinoa seeds in the passageway of the seed-filling room, which is reserved for the passage of the disturbed seed-filling mechanism, where the accumulation of seeds occurs. In order to determine the angular range of the position of the disturbed seed-filling mechanism, it is necessary to set up a monitoring point in the passageway to monitor the amount of seed in the passageway, as shown in Figure 7.

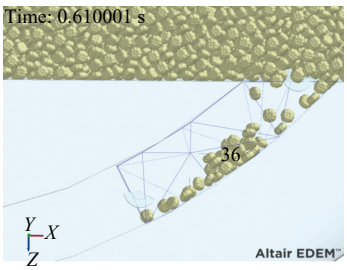

Figure 7 Seed number monitoring points

A second monitoring point is used for the monitoring of seeds on the disturbed seed-filling mechanism, as shown in Figure 8. The monitoring point is designed as a cylinder based on the movement process of the seed-metering device. The number of this monitoring point is 20, and it is set to rotate with the disturbed seed-filling mechanism. Whether the seed-filling table scoops up the seeds singly or not is used as the evaluation index, recorded as the I_q of scooping up the seeds, counted 50 times, and the average is taken.

Figure 8 Scooping monitoring point diagram

2.6 Experimental design of orthogonal simulation tests

Orthogonal tests are designed based on the range of levels of each factor screened in the single-factor test. According to the "Experimental Design and Data Processing" and related literature[22,23], orthogonal tests are designed according to the $L_9(3^4)$ orthogonal table. The orthogonal test factors are the GRDSM, the ADSM, and the PADSM, marked *A, B,* and *C,* respectively. Each factor is taken to three equal levels, and the test factors and levels are listed in Table 2.

Table 2 Experimental factors and levels

Level	Factor		
	GRDSM *A*/mm	ADSM *B*/(°)	PADSM *C*/(°)
1	1.2	120	20
2	1.3	140	25
3	1.4	160	30

2.7 Model pre-processing

To improve the speed of EDEM-Fluent coupling, the model needs to be simplified, and the fluid domain is divided into two in Fluent. The air chamber fluid domain is named "fluid1", and the seed-sucking hole fluid domain is named "fluid2". Meanwhile, the fluid domain of the seed-filling room needs to be added to the coupling simulation. Since the airflow has a less perturbing effect on the region far away from the seed-sucking hole, the perturbation of the seed population and the seed adsorption are concentrated around the seed-sucking hole, so the seed-filling room can be simplified into a cylinder[24,25]. The cylindrical fluid domain is named "fluid3", and the simplified model of each fluid domain is shown in Figure 9.

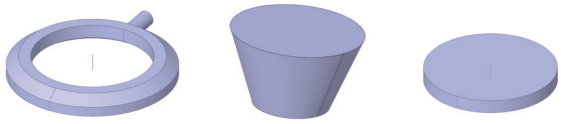

a. Fluid domain of air chamber b. Fluid domain of seed-sucking hole c. Fluid domain of seed-filling room

Figure 9 Schematic diagram of each fluid domain

2.8 EDEM coupling setup with Fluent

The EDEM simulation is divided into two phases twice: the first phase is seed stacking, and the second phase is the beginning of the rotation of the planter plate. After the seed stacking is completed, the results are exported. The coupling service is started in the EDEM toolbar after the start of the second phase of the simulation, followed by starting Fluent, loading the coupling interface, and setting it up in Fluent.

According to the working principle of the seed-metering device, the Fluent solution should be set as a transient solution. Since it is necessary to rotate the seed-sucking hole fluid domain using a slip mesh model, it should set up interfaces at four contact surfaces of the three fluid domains and name them "interface-1" (contact surface between the seed-sucking hole and the air chamber), "interface-2" (contact surface between the air chamber and the seed-sucking hole), "interface-3" (contact surface between

the seed-sucking hole and the seed-filling room), and "interface-4" (contact surface between the seed-filling room and the seed-sucking hole), respectively, in which interface-1 pairs up with interface-2, and interface-3 pairs up with interface-4, which is a total of 40 pairs. The rotational speed of the seed-sucking hole region in Fluent is set synchronously with the rotation speed of the planter plate in EDEM. The time step of EDEM is designed to be 3×10^{-6} s (about 19% of the Rayleigh time step), while the time step of Fluent is set to be 3×10^{-4} s (100 times the EDEM time step). The number of steps is set to 40 000, and other items are kept at the default settings[26-29].

2.9 Testing materials and equipment

The test is carried out by the requirements in "GB/T 6973-2005 Test Methods for Single Grain (Precision) Seeders". The test object is selected as Jili No. 3 quinoa seed, with a purity of 97% and without grading.

The test is conducted on the JPS-12 seed-metering device test-bench, and the test equipment and materials mainly include the drive gear, the seed-metering device, the positive pressure forced-draught fan, the positive pressure air tube, and the negative pressure air tube, as shown in Figure 10.

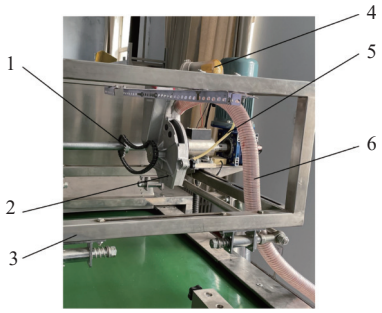

1. Drive gear 2. Seed-metering device 3. Step ping pedestal 4. Positive pressure forced-draught fan 5. Positive pressure air tube 6. Negative pressure air tube

Figure 10 Seed-metering device test-bench schematic diagram

2.10 Test evaluation indicators and test methods

To carry out a verification test on the seed-metering device with simulation design and parameterization, the test indices are selected as I_q, I_{mul}, and I_{miss} in this test, and the three working parameters of seed-sucking negative pressure, seed-metering device rotation speed, and seed-falling height are taken as the test factors to carry out the one-factor and response surface test. In the test, the theoretical grain spacing is taken as 15 cm. The data is recorded when the seed-metering device is running smoothly. The grain spacing distribution of 250 quinoa seeds is counted with the help of computerized image processing technology, the grain spacing data is exported after the seed spacing is detected, and the I_q, I_{mul}, and I_{miss} are calculated. Each group of tests is repeated three times, and the results are averaged.

2.11 Experimental design of response surface test

Before the response surface test, a single-factor pretest is conducted to determine the factor levels ranging from –2.5 kPa to –3.5 kPa for the seed-sucking negative pressure, 10-20 r/min for the seed-metering device rotation speed, and 50-150 mm for the seed-falling height. The test factor levels are listed in Table 3. The experimental design and results are listed in Table 4.

Table 3 Experimental factors and levels

Level	Factor		
	Seed-sucking negative pressure X_1/kPa	Seed-metering device rotation speed X_2/r·min^{-1}	Seed-falling height X_3/mm
–1	–2.5	10	50
0	–3.0	15	100
1	–3.5	20	150

Table 4 Experimental design and results

Test No.	X_1	X_2	X_3	Qualified index y_3/%	Miss index y_2/%	Multiple index y_3/%
1	1	1	0	75.0	10.5	14.5
2	0	0	0	80.0	8.5	11.5
3	0	0	0	81.5	8.5	10.0
4	–1	–1	0	73.5	9.0	17.5
5	0	1	–1	73.0	9.0	18.0
6	–1	0	1	68.0	8.5	23.5
7	0	–1	–1	75.0	13.0	12.0
8	0	1	1	71.0	8.0	21.0
9	1	0	1	76.5	11.0	12.5
10	0	0	0	83.0	7.0	10.0
11	0	0	0	81.0	7.5	11.5
12	–1	1	0	68.0	6.0	26.0
13	–1	0	–1	74.0	9.0	17.0
14	1	0	–1	73.5	15.5	11.0
15	0	–1	1	76.0	10.5	13.5
16	1	–1	0	78.0	14.0	8.0
17	0	0	0	80.0	8.0	12.0

3 Results and discussion

3.1 Fluent-based simulation results and analysis

3.1.1 Effect of different seed-sucking hole shapes and sizes on the flow field

Fluent is used to analyze the influence of six different shapes of seed-sucking holes, including cylindrical straight, conical angle-type, countersunk head bolt-type, diabolo-type, chamfer-type, and cone-frustum-type seed-sucking holes on the flow field of the air chamber. In this case, we consider defining the aperture of the taper hole and the circular-cone-type shape of the seed-sucking hole as the aperture of the smallest face, and setting the aperture to 1.2 mm. The inlet pressure magnitude is set to –3.0 kPa, and the other boundary conditions remain unchanged. A cross-section perpendicular to the seed-sucking holes is created in the post-processing module, and its pressure nephogram and velocity vectogram are shown in Figures 11 and 12.

From Figures 11 and 12, it can be seen that under the same negative pressure conditions, the surface negative pressure and flow rate of the cone-frustum-type seed-sucking holes are the largest. It shows that under the premise of being able to absorb the seeds, the seed-metering device with cone-frustum-type seed-sucking holes requires the least negative pressure provided by the forced-draught fan, which can greatly reduce the power consumption of the forced-draught fan. Therefore, the shape of the seed-sucking holes is chosen as cone-frustum-type. The seed-sucking hole size is mainly determined by two parameters: their inclination angle and their diameter. From Figures 11 and 12, the range of values for the diameter of seed-sucking holes is 0.8-1.6 mm, and the range of values for their inclination angle is set at 40°-80° based on the preliminary pre-tests.

In order to explore the influence of different inclination angles of seed-sucking holes on the flow field distribution in the air chamber, Fluent is used to analyze such influence under the condition that the diameter of the seed-sucking hole is set to 1.0 mm.

The legend range of the pressure nephogram is appropriately rounded based on the automatic range and is set to 10 Pa for each interval. The legend range of the velocity vectogram is set to 0-4 m/s. A cross section is created at 2 mm downward from the seed-sucking hole, and the pressure nephogram and velocity vectogram obtained are shown in Figures 13 and 14.

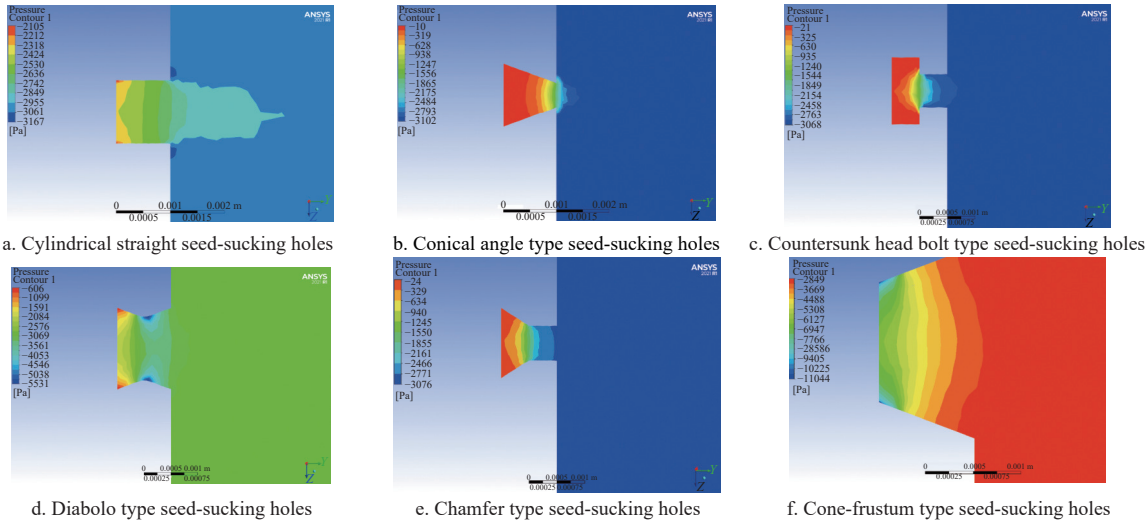

a. Cylindrical straight seed-sucking holes b. Conical angle type seed-sucking holes c. Countersunk head bolt type seed-sucking holes

d. Diabolo type seed-sucking holes e. Chamfer type seed-sucking holes f. Cone-frustum type seed-sucking holes

Figure 11 Pressure nephogram under different shapes of seed-sucking holes

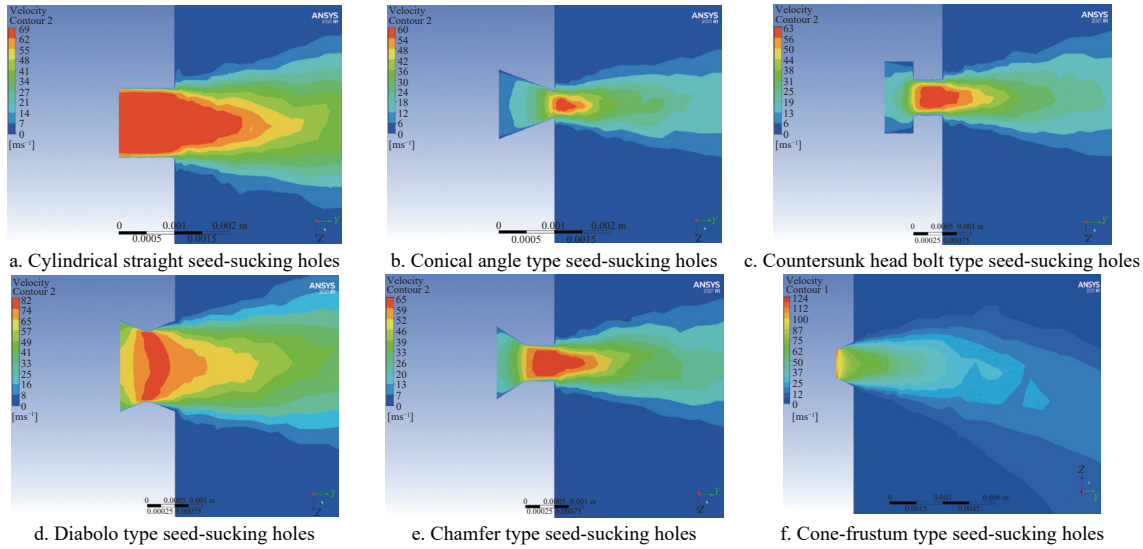

a. Cylindrical straight seed-sucking holes b. Conical angle type seed-sucking holes c. Countersunk head bolt type seed-sucking holes

d. Diabolo type seed-sucking holes e. Chamfer type seed-sucking holes f. Cone-frustum type seed-sucking holes

Figure 12 Velocity vectogram under different shapes of seed-sucking holes

Figure 13 can be analyzed from the point of view of the air chamber pressure value. When the inclination angle of the seed-sucking hole is 40°-70°, the air chamber pressure value decreases gradually. When the inclination angle of the seed-sucking hole is 80°, the air chamber pressure value increases slightly. According to Figure 14, from the analysis of the distribution of the larger vector of velocity, it can be seen that when the inclination angle of the seed-sucking hole is 80°, the value of the pressure in the air chamber is larger. According to the relationship between the pressure and the flow rate, it can be seen that the flow rate at this time should be smaller. When the inclination angle of the seed-sucking hole is 70°, the air occupies the full air chamber at a faster speed. In order to further obtain the optimal inclination angles of the seed-sucking holes, the negative pressure average of each seed-sucking hole in the seed-filling area and the standard deviation of the negative pressure value of each seed-sucking hole in the seed-carrying area are output through the Report module in Fluent, as listed in Table 5.

As can be seen from Table 5, the average value of negative pressure in the seed-filling area increases and then decreases with the increase in the inclination angles of the seed-sucking holes. The average value of negative pressure in the seed-filling area reaches its maximum value when the inclination angle of the seed-sucking hole is 70°.

Table 5 Simulation results under different inclination angles of seed-sucking holes

Inclination angle of seed-sucking hole/(°)	Negative pressure average of each seed-sucking hole in the seed-filling area	Standard deviation of negative pressure of each seed-sucking hole in the seed-carrying area
40	3505.67	36.63
50	3842.09	7.84
60	5252.04	10.64
70	7415.82	14.39
80	5775.72	17.36

By comprehensively considering the pressure distribution of the air chamber, the distribution of velocity vectors, the negative pressure average of each seed-sucking hole in the seed-filling area, and the standard deviation of the negative pressure value of each

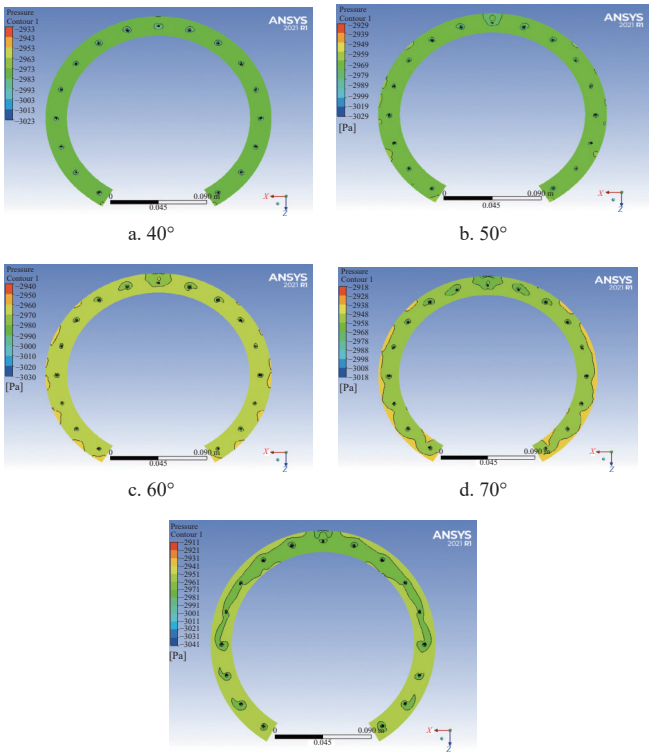

a. 40° b. 50°

c. 60° d. 70°

e. 80°

Figure 13 Pressure nephogram under different inclination angles of seed-sucking holes

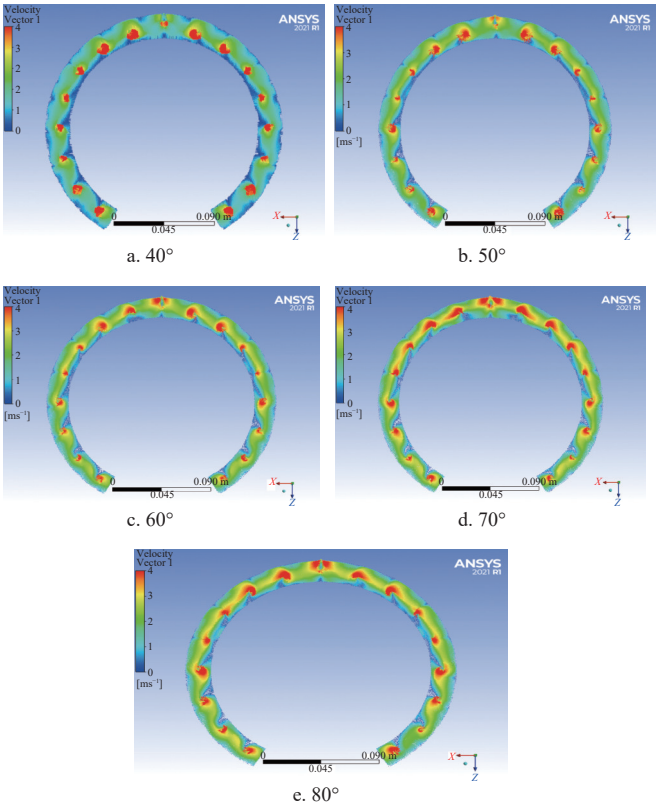

a. 40° b. 50°

c. 60° d. 70°

e. 80°

Figure 14 Velocity vectogram under different inclination angles of seed-sucking holes

seed-sucking hole in the seed-carrying area, the inclination angle of the seed-sucking hole is finally determined to be 70°. According to the above analysis, it can be seen that under the condition that the inclination angle of the seed-sucking hole is 70° and other parameters are the same, the flow field distribution of the air chamber under five different diameters of the seed-sucking holes (0.8 mm, 1.0 mm, 1.2 mm, 1.4 mm, and 1.6 mm) is analyzed by Fluent. Following the same setup, the pressure nephogram and velocity vectogram of the air chamber are obtained, as shown in Figures 15 and 16.

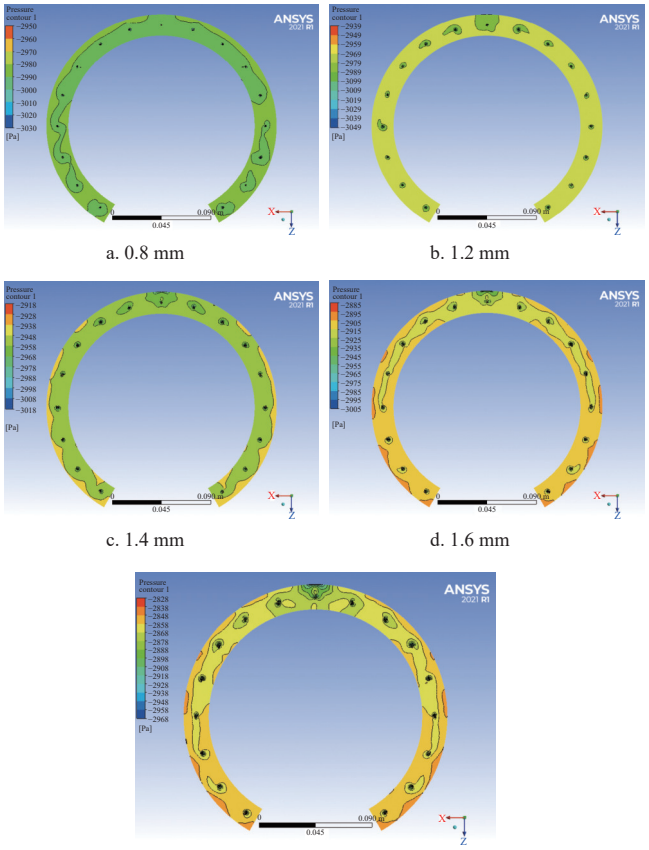

a. 0.8 mm b. 1.2 mm

c. 1.4 mm d. 1.6 mm

e. 1.6 mm

Figure 15 Pressure nephogram under different diameters of seed-sucking holes

According to Figure 15, the pressure stratification is most prominent in the seed-sucking holes with diameters of 1.4 mm and 1.6 mm. Analyzing from the point of view of the pressure value in the air chamber, the pressure inside the air chamber decreases gradually with the increase of the diameter of the seed-sucking hole. According to Figure 16, it is more obvious when the diameter of the seed-sucking hole is 1.0-1.6 mm, which indicates that the time required for the air to occupy the air chamber is gradually shortened. In order to further obtain the optimal diameter of the seed-sucking holes, the negative pressure average of each seed-sucking hole in the seed-filling area and the standard deviation of the negative pressure value of each seed-sucking hole in the seed-carrying area are output through the Report module in Fluent, as listed in Table 6.

As shown in Table 6, the average negative pressure of each seed-sucking hole in the seed-filling area increased and then decreased with the increase in the diameters of the seed-sucking holes. The standard deviation of the negative pressure value of each seed-sucking hole in the seed-carrying area decreased then increased and then decreased again. Considering the pressure distribution of the air chamber, the distribution of velocity vectors, the average negative pressure of each seed-sucking hole in the seed-filling area, and the standard deviation of negative pressure values of each seed-sucking hole in the seed-carrying area, the diameter of the seed-sucking holes was finally determined to be 1.0 mm.

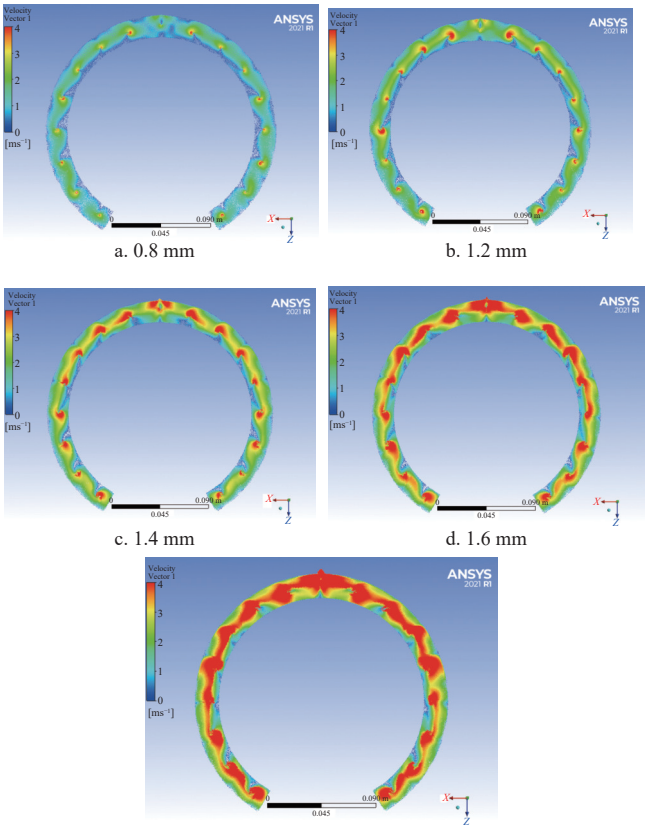

a. 0.8 mm b. 1.2 mm

c. 1.4 mm d. 1.6 mm

e. 1.6 mm

Figure 16 Velocity vectogram under different diameters of seed-sucking holes

Table 6 Simulation results under different diameters of seed-sucking holes

Diameter of seed-sucking hole/mm	Negative pressure average of each seed-sucking hole in the seed-filling area	Standard deviation of negative pressure value of each seed-sucking hole in the seed-carrying area
0.8	7604.64	212.55
1.0	7692.65	22.72
1.2	7415.81	14.97
1.4	7089.65	24.31
1.6	6795.93	16.14

3.1.2 Effect of different seed-sucking hole numbers on the flow field

The number of seed-sucking holes also has a significant impact on the efficiency of the seed-metering device. Based on the above analysis, the simulation is carried out for five different numbers of seed-sucking holes, such as 12, 20, 28, 36, and 44, with a 70° inclination angle of the seed-sucking hole, a 1.0 mm diameter of the seed-sucking hole, and a 15 r/min rotation speed of the seed-metering device. The pressure nephogram and velocity vectogram are obtained as shown in Figures 17 and 18.

According to Figure 17, the uniformity of the pressure distribution inside the air chamber increases and then decreases with the increase in the number of seed-sucking holes. The pressure distribution inside the air chamber is most uniform when the number of seed-sucking holes is 20. According to Figure 18, it can be seen that with the increase of the number of seed-sucking holes, the vector with larger velocity inside the air chamber gradually increases, and it is more obvious when the number of seed-sucking holes is 36-44, which indicates that the time required for air to occupy the air chamber is gradually shortened. In order to further

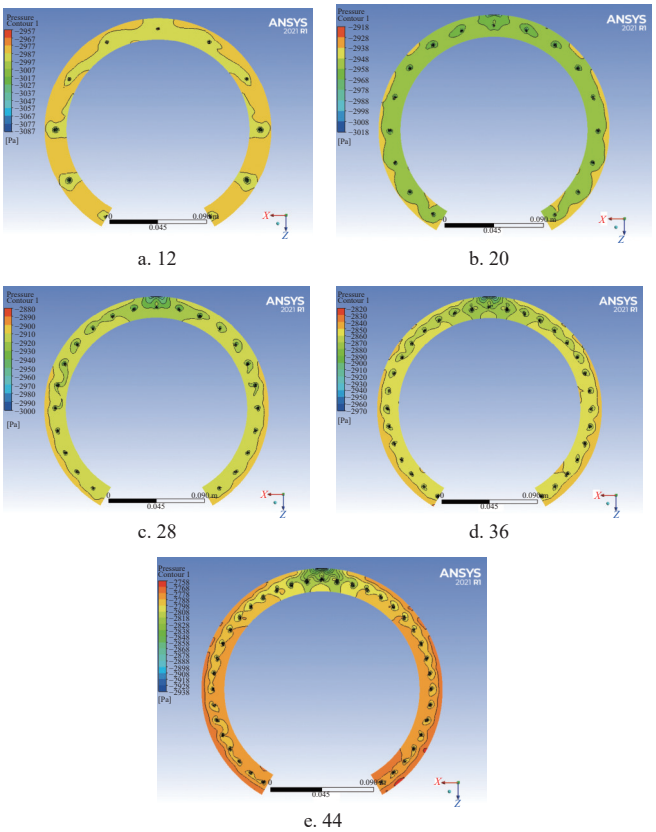

a. 12 b. 20

c. 28 d. 36

e. 44

Figure 17 Pressure nephogram under different number of seed-sucking holes

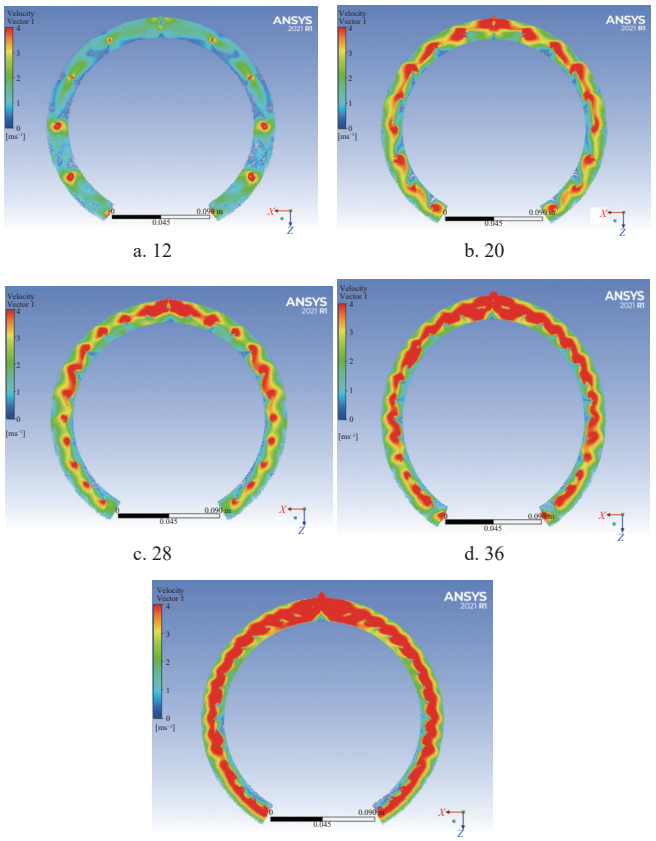

a. 12 b. 20

c. 28 d. 36

e. 44

Figure 18 Velocity vectogram under different number of seed-sucking holes

obtain the optimal number of seed-sucking holes, the negative pressure average of each seed-sucking hole in the seed-filling area

and the standard deviation of the negative pressure value of each seed-sucking hole in the seed-carrying area is output through the Report module in Fluent, as listed in Table 7.

Table 7 Simulation results under number of seed-sucking holes

Number of seed-sucking holes/mm	Negative pressure average of each seed-sucking hole in the seed-filling area	Standard deviation of negative pressure value of each seed-sucking hole in the seed-carrying area
12	7497.88	28.72
20	7415.81	14.39
28	7253.57	21.63
36	7129.73	22.02
44	6935.69	42.89

As can be seen from Table 7, the average negative pressure of each seed-sucking hole in the seed-filling area gradually decreases, and the standard deviation of the negative pressure value of each seed-sucking hole in the seed-carrying area first decreases and then increases with the increase in the number of seed-sucking holes. When the number of seed-sucking holes is 20, the standard deviation of the negative pressure value of each seed-sucking hole in the seed-carrying area is the smallest, and the movement of seeds in the seed-carrying area is more stable. The number of seed-sucking holes is determined to be 20 by considering the pressure distribution in the air chamber, the distribution of velocity vectors, the negative pressure average of each seed-sucking hole in the seed-filling area, and the standard deviation of the negative pressure value of each seed-sucking hole in the seed-carrying area.

3.2 EDEM-based simulation results analysis

The evaluation index for the test is the scooping I_q, calculated by the following equation:

$$Y = \frac{Y_1}{Y_2} \tag{9}$$

where, Y is the scooping I_q, %; Y_1 is the number of individual seeds scooped up on the disturbed seed-filling mechanism; and Y_2 is the total number of scooping times on the disturbed seed-filling mechanism.

3.2.1 Results analysis of single-factor simulation test

Under the condition that the ADSM is 140° and the PADSM is 30°, the effects of five different notch radii, namely 1.1 mm, 1.2 mm, 1.3 mm, 1.4 mm, and 1.5 mm, on the performance of seed-scooping are analyzed using the EDEM software. Through the post-processing module of EDEM, we can see that the I_q of seed-scooping decreases and then increases with the increase in the notch radius. At the same time, if the radius of the notch is small, the seeds fly out directly from the arc edge of the disturbed seed-filling mechanism, resulting in seed-scooping failure. When the radius of the notch is large, the phenomenon of scooping multiple seeds on the disturbed seed-filling mechanism also occurs, which affects the subsequent seed-filling. Based on the above analysis, the horizontal range of the notch radius in the subsequent orthogonal test is designed as 1.2-1.4 mm.

Under the condition that the GRDSM is 1.3 mm and the PADSM is 30°, the effects of five different position angles of the disturbed seed-filling mechanism, namely 100°, 120°, 140°, 160°, and 180°, on the seed-scooping performance are analyzed by EDEM software. Through the post-processing module of EDEM to count the seed-scooping I_q of the monitoring points, it can be found that with the increase in the ADSM, the seed-scooping I_q increases first and then decreases. This means that when the ADSM is too small, the contact chance and contact area between seeds and the disturbed seed-filling mechanism are small, and the seeds are not easy to scoop up. When the ADSM is too large, the contact chance and contact area between seeds and the disturbed seed-filling mechanism are large, and there may be a case of filling multiple seeds in the groove, which affects the subsequent seed-filling. Based on the above analysis, the horizontal range of the ADSM in the subsequent orthogonal test is designed as 120°-160°.

Under the condition that the GRDSM is 1.3 mm and the ADSM is 140°, the effects of five different position angles of the disturbed seed-filling mechanism, namely 20°, 25°, 30°, 35°, and 40°, on the seed-scooping performance are analyzed by EDEM software. It can be observed that with the increase in the position angles of the disturbed seed-filling mechanism, the I_q of seed-scooping increases first and then decreases. Meanwhile, when the angle in the position of the disturbed seed-filling mechanism is too small, the seed-scooping capacity of the disturbed seed-filling mechanism is low and cannot scoop up the seeds. When the position angles of the disturbed seed-filling mechanism are too large, the seeds will be stuck at the bottom of the disturbed seed-filling mechanism, and it is not easy for the seeds to enter the grooves. Based on the above analysis, the horizontal range of the position angles of the disturbed seed-filling mechanism in the subsequent orthogonal test is designed as 20°-30°.

3.2.2 Results analysis of orthogonal simulation tests

The orthogonal test factors are the GRDSM, the ADSM, and the PADSM, marked *A*, *B,* and *C*, respectively. To reduce random errors and increase reliability, a blank column is inserted, which is marked D. Each factor is taken to three equal levels, which are marked 1, 2, and 3, respectively. The test factors and levels are shown in Table 2. The orthogonal simulation tests are listed in Table 8.

Table 8 Orthogonal experimental results

Serial No.	Factor level value				I_q of scooping seeds/%
	A	*B*	*C*	D	
1	1	1	1	1	64
2	1	2	2	2	76
3	1	3	3	3	66
4	2	1	2	3	80
5	2	2	3	1	78
6	2	3	1	2	68
7	3	1	3	2	72
8	3	2	1	3	72
9	3	3	2	1	74

The results of the orthogonal test are analyzed for range analysis as listed in Table 9 and variance analysis as listed in Table 10.

Table 9 Range analysis of orthogonal test results

Analysis item	*A*	*B*	*C*	*D*
*K*1	206	216	204	216
*K*2	226	226	230	216
*K*3	218	208	216	218
*k*1	68.67	72	68	72
*k*2	75.33	75.33	76.67	72
*k*3	72.67	69.33	72	72.67
R	6.67	6	8.67	0.67
Factor priority	*C*>*A*>*B*>*D*			
Better combination	$A_2B_2C_2$			

Table 10 Variance analysis of orthogonal test results

Source	Freedom	Sum of squares	Mean square	*F* value	*p*-value	Significance
A	2	67.56	33.78	76	0.013	*
B	2	54.22	27.11	61	0.016	*
C	2	112.89	56.44	127	0.009	**
Error	2	0.89	0.44	-	-	-

Note: * indicates significant difference (p<0.05); ** indicates highly significant difference (p<0.01).

According to Table 10, it can be seen that the effect of the PADSM on the seed-scooping I_q is highly significant. The comprehensive analysis shows that the best combination is as follows: 1.3 mm GRDSM, 140° groove ADSM, 25° PADSM.

3.3 EDEM-Fluent coupling-based simulation results analysis

Under the same rotational speed and negative pressure conditions, simulation and comparison tests are carried out on the air-suction-type seed-metering device with or without a disturbed seed-filling mechanism. After counting the seed-sucking situation of 50 seeds, the I_q of the seed-metering device with or without a disturbed seed-filling mechanism are 80% and 72%, respectively. This indicates that the design of the disturbed seed-filling mechanism could improve the uniformity in the seeding of the seed-metering device.

3.4 Response surface test results analysis

3.4.1 Variance analysis

From Table 4, the regression equations of I_q, I_{mul}, and I_{miss} can be obtained as shown in Equations (10)-(12). The variance analysis tables (Tables 11, 12, and 13) for the I_q, I_{miss}, and I_{mul} show that the p-values of the three models are 0.0001, not more than 0.0001, and not more than 0.0001, respectively, and they are all less than 0.05, so the differences are significant. The p-values of the three misfit terms are 0.7037, 0.3533, and 0.8613, respectively, which are all greater than 0.05, and so the difference is not significant. They indicate that the regression equations can fit the real experimental results better[30-33].

$$y_1 = 81.1 + 2.44X_1 - 1.94X_2 - 0.5X_3 + 0.625X_1X_2 + 2.25X_1X_3 - 0.75X_2X_3 - 4.11X_1^2 - 3.36X_2^2 - 3.99X_3^2 \quad (10)$$

$$y_2 = 11 - 4.75X_1 + 3.56X_2 + 1.56X_3 - 0.5X_1X_2 - 1.25X_1X_3 + 0.375X_2X_3 + 2.69X_1^2 + 2.81X_2^2 + 2.31X_3^2 \quad (11)$$

$$y_3 = 7.9 + 2.31X_1 - 1.63X_2 - 1.06X_3 - 0.125X_1X_2 - X_1X_3 + 0.375X_2X_3 + 1.42X_1^2 + 0.55X_2^2 + 1.68X_3^2 \quad (12)$$

The experimental results are analyzed using Design-Expert 13 software to obtain the variance analysis of the I_q, the I_{miss}, and the I_{mul}.

From the variance analysis of the regression equations of each model, the effect of X_3, X_1X_2, and X_2X_3 on the y_1 model (I_q) is not significant. The effect of X_1X_2 as well as X_2X_3 on the y_2 model (I_{miss}) is not significant, and the effect of X_2X_2, X_1X_2, and X_2X_3 on the y_3 model (I_{mul}) is not significant. The model after the elimination of insignificant terms is:

$$y_1 = 81.1 + 2.44X_1 - 1.94X_2 + 2.25X_1X_3 - 4.11X_1^2 - 3.36X_2^2 - 3.99X_3^2 \quad (13)$$

$$y_2 = 11 - 4.75X_1 + 3.56X_2 + 1.56X_3 - 1.25X_1X_3 + 2.69X_1^2 + 2.81X_2^2 + 2.31X_3^2 \quad (14)$$

$$y_3 = 7.9 + 2.31X_1 - 1.63X_2 - 1.06X_3 - X_1X_3 + 1.42X_1^2 + 0.55X_2^2 \quad (15)$$

Table 11 Variance analysis of the I_q

Source	Freedom	Sum of squares	Mean square	*F* value	*p*-value	Significance
Mode	9	311.02	34.56	28.42	0.0001	**
X_1	1	47.53	47.53	39.09	0.0004	**
X_2	1	30.03	30.03	24.70	0.0016	**
X_3	1	2.00	2.00	1.64	0.2405	-
X_1X_2	1	1.56	1.56	1.28	0.2943	-
X_1X_3	1	20.25	20.25	16.65	0.0047	**
X_2X_3	1	2.25	2.25	1.85	0.2159	-
X_1^2	1	71.21	71.21	58.56	0.0001	**
X_2^2	1	47.61	47.61	39.15	0.0004	**
X_3^2	1	66.95	66.95	55.05	0.0001	**
Residual error	7	8.51	1.22	-	-	-
Lack of fit	3	2.31	0.7708	0.4973	0.7037	-
Pure Error	4	6.20	1.55	-	-	-
Cor total	16	319.53	-	-	-	-

Note: * indicates significant difference (p<0.05); ** indicates highly significant difference (p<0.01).

Table 12 Variance analysis of the I_{miss}

Source	Freedom	Sum of Squares	Mean Square	*F* value	*p*-value	Significance
Mode	9	405.66	45.07	43.15	<0.0001	**
X_1	1	180.50	180.50	172.79	<0.0001	**
X_2	1	101.53	101.53	97.19	<0.0001	**
X_3	1	19.53	19.53	18.70	0.0035	**
X_1X_2	1	1.0000	1.0000	0.9573	0.3605	-
X_1X_3	1	6.25	6.25	5.98	0.0444	*
X_2X_3	1	0.5625	0.5625	0.5385	0.4869	-
X_1^2	1	30.41	30.41	29.11	0.0010	**
X_2^2	1	33.31	33.31	31.88	0.0008	**
X_3^2	1	22.52	22.52	21.55	0.0024	**
Residual error	7	7.31	1.04	-	-	-
Lack of fit	3	3.81	1.27	1.45	0.3533	-
Pure error	4	3.50	0.8750	-	-	-
Cor total	16	412.97	-	-	-	-

Note: * indicates significant difference (p<0.05); ** indicates highly significant difference (p<0.01).

Table 13 Variance analysis of the I_{mul}

Source	Freedom	Sum of Squares	Mean Square	*F* value	*p*-value	Significance
Mode	9	101.25	11.25	39.13	< 0.0001	**
X_1	1	42.78	42.78	148.80	< 0.0001	**
X_2	1	21.13	21.13	73.48	< 0.0001	**
X_3	1	9.03	9.03	31.41	0.0008	**
X_1X_2	1	0.0625	0.0625	0.2174	0.6552	-
X_1X_3	1	4.00	4.00	13.91	0.0074	**
X_2X_3	1	0.5625	0.5625	1.96	0.2046	-
X_1^2	1	8.55	8.55	29.74	0.0010	**
X_2^2	1	1.27	1.27	4.43	0.0733	-
X_3^2	1	11.81	11.81	41.09	0.0004	**
Residual error	7	2.01	0.2875	-	-	-
Lack of fit	3	0.3125	0.1042	0.2451	0.8613	-
Pure Error	4	1.70	0.4250	-	-	-
Cor total	16	103.26	-	-	-	-

Note: *indicates significant difference (p<0.05); **indicates highly significant difference (p<0.01).

3.4.2 Response surface analysis

Response surface analysis is carried out by Design-Expert software to obtain the effects of the interaction between the seed-sucking negative pressure, the seed-metering device rotation speed, and the seed-falling height on the I_q, I_{miss}, and I_{mul}. The response surface plot is the output. The effect on I_q is shown in Figure 19.

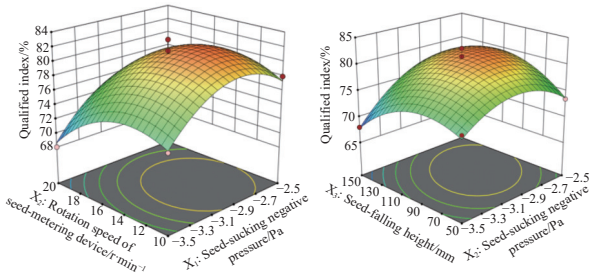

a. Effect of seed-metering device rotation speed and seed-sucking negative pressure on Iq

b. Effect of seed-falling height and seed-sucking negative pressure on Iq

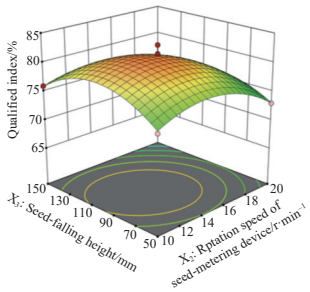

c. Effect of seed-metering device rotation speed and seed-falling height on Iq

Figure 19 Effect of interaction on I_q

From Figure 19a, it can be seen that when the seed-sucking negative pressure is –2750 to –3250 Pa and the seed-metering device rotation speed is 12.5-17.5 r/min, the I_q of the seed-metering device is higher. When fixing one of the two factors (seed-metering device rotation speed and seed-sucking negative pressure), the I_q increases and then decreases with the increase in the other factor. As can be seen from Figure 19b, when the seed-falling height is 75-125 mm and the seed-sucking negative pressure is –2750 to –3250 Pa, the I_q of the seed-metering device is higher. When one of the two factors of seed-falling height and seed-sucking negative pressure is fixed, the I_q increases and then decreases with the increase in the other factor. From Figure 19c, it can be seen that the I_q of the seed-metering device is higher when the seed-falling height is 75-125 mm and the seed-metering device rotation speed is 12.5-17.5 r/min. When fixing one of the two factors of the seed-metering device rotation speed and seed-falling height, the I_q increases and then decreases with the increase of the other factor.

The effect of the interaction between the seed-sucking negative pressure, the seed-metering device rotation speed, and the seed-falling height on the I_{miss} is shown in Figure 20.

From Figure 20a, it can be seen that the I_{miss} of the seed-metering device is lower when the seed-metering device rotation speed is 12.5-17.5 r/min and the seed-sucking negative pressure is –2750 to –3250 Pa. When one of the two factors (seed-metering device rotation speed and seed-sucking negative pressure) is fixed, the I_{miss} increases with the increase of the seed-metering device rotation speed and decreases with the increase of seed-sucking negative pressure. From Figure 20b, it can be seen that the I_{miss} of the seed-metering device is lower when the seed-falling height is 75-125 mm and the seed-sucking negative pressure is –2750 to –3250 Pa. When one of the two factors, seed-falling height and seed-sucking negative pressure, is fixed, the I_{miss} increases with the increase of seed-falling height and decreases with the increase of seed-sucking negative pressure. From Figure 20c, it can be seen that the I_{miss} of the seed-metering device is lower when the seed-falling height is 75-125 mm and the seed-metering device rotation speed of the seed-metering device is 12.5-17.5 r/min. When fixing one of the two factors of seed-metering device rotation speed and seed-falling height, the I_{miss} increases with the increase of the other factor.

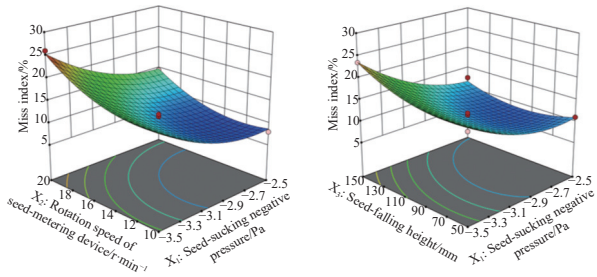

a. Effect of seed-metering device rotation speed and seed-sucking negative pressure on I_{miss}

b. Effect of seed-falling height and seed-sucking negative pressure onImiss

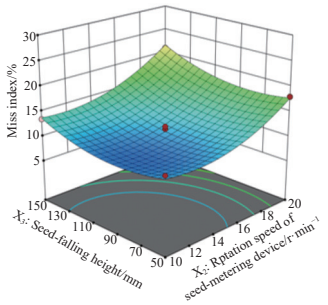

c. Effect of seed-metering device rotation speed and seed-falling height on Imiss

Figure 20 Effect of interaction on I_{miss}

The effect of the interaction between seed-sucking negative pressure, seed-metering device rotation speed, and seed-falling height on the I_{mul} is shown in Figure 21.

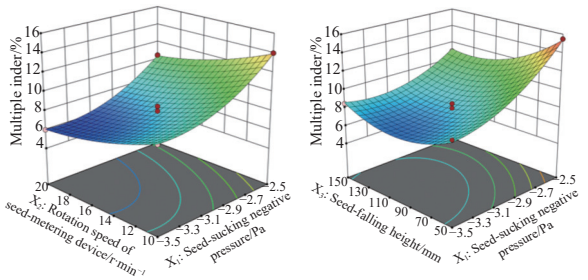

a. Effect of seed-metering device rotation speed and seed-sucking negative pressure on I_{mul}

b. Effect of seed-falling height and seed-sucking negative pressure on I_{mul}

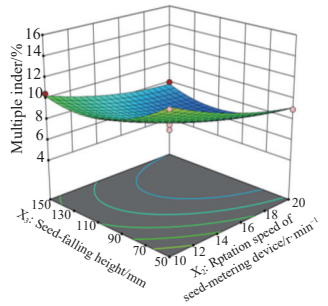

c.Effect of seed-metering device rotation speed and seed-falling height on I_{mul}

Figure 21 Effect of interaction on I_{mul}

As can be seen in Figure 21a, the I_{mul} of the seed-metering device is lower when the seed-metering device rotation speed is 12.5-17.5 r/min and the seed-sucking negative pressure is –2750 to –3250 Pa. When one of the two factors (seed-metering device rotation speed and seed-sucking negative pressure) is fixed, the I_{mul} decreases with the increase of the seed-metering device rotation speed and increases with the increase of seed-sucking negative pressure. As can be seen from Figure 21b, the I_{mul} of the seed-metering device is lower when the seed-falling height is 75-125 mm and the seed-sucking negative pressure is –2750 to –3250 Pa. When one of the two factors of seed-falling height and seed-sucking negative pressure is fixed, the I_{mul} decreases with the increase of seed-falling height and increases with the increase of seed-sucking negative pressure. From Figure 21c, it can be seen that the I_{mul} of the seed-metering device is lower when the seed-falling height is 75-125 mm and the seed-metering device rotation speed is 12.5-17.5 r/min. When fixing one of the two factors of seed-metering device rotation speed and seed-falling height, the I_{mul} decreases with the increase of the other factor.

3.5 Verification test

By constraining the above regression equations, the following functions can be obtained:

$$\begin{cases} \max y_1(X_1, X_2, X_3) \\ y_2(X_1, X_2, X_3) < 10\% \\ y_3(X_1, X_2, X_3) < 20\% \\ \text{s.t.} \begin{cases} -3.5 < X_1 < -2.5 \\ 10 < X_2 < 20 \\ 50 < X_3 < 150 \end{cases} \end{cases} \tag{16}$$

After solving Equation (16), the optimal combination of parameters is obtained as follows: –3.0 kPa seed-sucking negative pressure, 15 r/min seed-metering device rotation speed, and 100 mm seed-falling height. The results of the verification test are carried out on the optimized parameters, and the test results are as follows: the I_q is 82.5%, the I_{miss} is 6.5%, and the I_{mul} is 11%. The test results meet the index requirements in "JB/T 10293–2013 Technical Conditions of Single Seed (Precision) Seeder": the I_q is not less than 75%, the I_{miss} is not more than 10%, and the I_{mul} is not more than 20%.

4 Conclusions

(1) In this study, a positive-negative pressure quinoa precision seed-metering device with a disturbed seed-filling mechanism is designed. The key structure and parameters of the seed-metering device are designed, the diameter of the planter plate is determined to be 220 mm, and the radius of the distribution circle of the seed-sucking hole is 95 mm. The passageway is an asymmetric structure which is 5 mm above and 3 mm below the seed-sucking hole distribution circle. The above research content provides a basis for the simulation analysis of the subsequent seed-metering device.

(2) Fluent 2021 R1 simulation software is used to simulate and analyze the distribution of the flow field in the air chamber of the seed-metering device. The ideal combinations of the seed-sucking hole parameters are obtained through the single-factor simulation test: the shape of the seed-sucking hole is a circular-cone-type shape, the number of seed-sucking holes is 20, the inclination angle of the seed-sucking hole is 70°, and the diameter of the seed-sucking hole is 1.0 mm.

(3) The structure of the disturbed seed-filling mechanism is designed using EDEM 2020 simulation software. The optimal combinations of the structural parameters of the disturbed seed-filling mechanism are obtained through the simulation of orthogonal tests: 1.3 mm GRDSM, 140° ADSM, and 25° PADSM. The coupled EDEM-Fluent simulation shows that the design of the disturbed seed-filling mechanism improves the uniformity of seeding in the seed-metering device.

(4) With the help of the JPS-12 seed-metering device test-bench, a response surface test is carried out to analyze the effects of seed-sucking negative pressure, seed-metering device rotation speed, and seed-falling height on the I_q, the I_{miss}, and the I_{mul}. The optimal parameter combinations are obtained: –3.0 kPa seed-sucking negative pressure, 15 r/min seed-metering device rotation speed, and 100 mm seed-falling height. The optimized parameters are verified, and the results are: 82.5% I_q, 6.5% I_{miss}, and 11% I_{mul}, which meet the requirements of "JB/T 10293–2013 Technical Conditions of Single Seed (Precision) Seeder".

Acknowledgements

This work was financially supported by Key R&D Program of Hebei (Grant No. 21326305D, 21327215D), Local Science and Technology Development Fund Projects Guided by the Central Government (Grant No. 236Z7202G), and Zhangjiakou Significant Scientific and Technical Achievement Transformation Project (Grant No. 2311012Hc).

[References]

[1] Qiu Z M, Zhang W P, Zhao B, Ji J T, Jin X, He Z T. Design and test of operation quality monitoring system for small grain electric seeder. Transactions of the CSAM, 2019; 50(4): 77–83. (in Chinese)

[2] Du J W, Yang X J, Liu L J, Zhao J H, Zhao Z B. Research status and development trend of precision seeder for small seeds. Agricultural Engineering, 2017; 7(6): 9–13. (in Chinese)

[3] Zhang K, Hong Y, Xu Z X. Simulation of an air suction seed drainer based on DEM-CFD coupling. Journal of Nanjing University of Information Science & Technology, 2020; 12(6): 767–772. (in Chinese)

[4] Zhu J J, Liu J, Fu Y B, XI Y Y. Experimental study on performance of seed discharging device of air-suction precision cave-sowing machine. Journal of Agricultural University of Hebei, 2021; 44(4): 115–118. (in Chinese)

[5] Wang F Y, Yang L, Wang H T. Design and Test of Electric Driving Pneumatic Carrot Planter in Greenhouse. Transactions of the CSAM, 2022; 53(8): 64–73. (in Chinese)

[6] Zeng S, Yao L M, Li N, Yang Y K, Huang D P, Fang L Y, Mo Z W. Development and test of an air-suction type precision direct seeding machine for pepper. Journal of South China Agricultural University, 2020; 41(3): 102–109. (in Chinese)

[7] Yi S J, Chen T, Li Y F, Tao G X, Mao X. Design and test of millet hill-drop seed-metering device with combination of positive-negative pressure and hole wheel. Transactions of the CSAM, 2021; 52(6): 83–94. (in Chinese)

[8] Liao Y T, Zheng J, Liao Q X, Ding Y C, Gao L P. Design and experiment of positive and negative pressure combined tube-needle centralized seeding device for American ginseng. Transactions of the CSAM, 2019; 50(3): 46–57. (in Chinese)

[9] Abdolahzare Z, Mehdizadeh S A. Nonlinear mathematical modeling of seed spacing uniformity of a pneumatic planter using genetic programming and image processing. Neural Computing and Applications, 2018; 29(2): 363–375.

[10] Singh R C, Singh G, Saraswat D C. Optimisation of design and operational parameters of a pneumatic seed metering device for planting cottonseeds. Biosystems Engineering, 2005; 92(4): 429–438.

[11] Liao Y T, Wang L, Liao Q X. Design and test of an inside-filling pneumatic precision centralized seed-metering device for rapeseed. Int J Agric & Biol Eng, 2017; 10(2): 56–62.

[12] Liao Y T, Liao Q X, Wang L, Zheng J, Gao L P. Investigation on vacuum singulating effect influencing factors of pneumatic precision seed metering device for small particle size of seeds. Transactions of the CSAE, 2018;

34(24): 10–17. (in Chinese)
[13] Wang G W, Xia X M, Zhu Q H, Yu H Y, Huang D Y. Design and test of high-speed precision seed dispenser for soybean based on DEM-CFD coupling with auxiliary seed filling air suction. Journal of Jilin University (Engineering Edition), 2022; 52(5): 1208–1221. (in Chinese)
[14] Wu F T. Research on positive and negative air pressure combination of rapeseed precision direct seeding rower. Huazhong Agricultural University, 2008. (in Chinese)
[15] Zhang K X, Li J F, Song Z H, Liu X X, Liu L. Optimum design and test of variable diameter double disc air suction precision seeder. Transactions of the CSAM, 2019; 50(6): 52–63.
[16] Shi R J, Dai F, Zhao W Y, Yang F R, Zhang F W, Zhao Y M, et al. Design and experiments of self-propelled quinoa combine harvester. Journal of Jilin University (Engineering and Technology Edition), 2023; 53(9): 2686–2694. (in Chinese)
[17] Cao L X, Zhou H T, Li T L, Shi B H, Zhang L X, Zhang X J, et al. Selection and development of a highly collapse-resistant quinoa cultivar, Ji Quinoa 3, and light simplified cultivation technology. Agricultural Science and Technology Newsletter, 2021; 11: 261–263, 289. (in Chinese)
[18] Hu M, Xia J, Zhou Y, Luo C, Zhou M, Liu Z. Measurement and calibration of the discrete element parameters of coated delinted cotton seeds. Agriculture, 2022; 12(2): 286.
[19] Li Z D, Yang W C, Zhang T, Wang W W, Zhang S, Chen L Q. Design and suction performance test of sucking-seed plate combined with groove-tooth structure on high speed precision metering device of rapeseed. Transactions of the CSAE, 2019; 35(1): 12–22. (in Chinese)
[20] Yang H, Cao M, Wang B, Hu Z, Xu H, Wang S, Yu Z. Design and test of a tangential-axial flow picking device for peanut combine harvesting. Agriculture, 2022; 12(2): 179.
[21] He R Y, Wang J L, Xu G M, He X Y, Duan Q F, Ding Q S. Design and experiment of wheat precise seed metering apparatus with positive and negative pressure with function of limiting seed filling posture. Transactions of the CSAM, 2022; 53(9): 39–49, 167. (in Chinese)
[22] Bai W J, Li Y, Yu H L, Zhao D W, Li X L, Zhao X S. Design and simulation optimization of positive and negative pressure seed-metering device. Journal of Hebei Agricultural University, 2022; 45(4): 115–122. (in Chinese)
[23] Wang X Y, Kang J M, Ding H F, Peng Q J, Zhang C Y, Li N N. Design and test of 2BM-4 film mulch precision planter for quinoa. Transactions of the CSAM, 2020; 51(12): 86–94. (in Chinese)
[24] Zhao X S, Ran W J, Hao J J, Bai W J, Yang X L. Design and experiment of the double-seed hole seeding precision seed metering device for peanuts. Int J Agric & Biol Eng, 2022; 15(3): 107–114.
[25] Wang G W, Xia X M, Zhu Q H, Yu H Y, Huang D Y. Design and experiment of soybean high-speed precision vacuum seed metering with auxiliary filling structure based on DEM-CFD. Journal of Jilin University (Engineering and Technology Edition), 2022; 52(5): 1208–1221.
[26] Li Y M, Chandio F A, Ma Z, Lakhiar I A, Sahito A R, Ahmad F, et al. Mechanical strength of wheat grain varieties influenced by moisture content and loading rate. Int J Agric & Biol Eng, 2018; 11(4): 52–57.
[27] Ibrahim E J, Liao Q X, Lei W, Liao Y T, Lu Y. Design and experiment of multi-row pneumatic precision metering device for rapeseed. Int J Agric & Biol Eng, 2018; 11(5): 116–123.
[28] Cheng B, He R, Xu Y, Zhang X. Simulation analysis and test of pneumatic distribution fertilizer discharge system. Agronomy, 2022; 12(4): 2282.
[29] Feng Y B, Zhao X S, Li J C, Yu H L, Zhao H P, Yin B Z. Parameter optimization and experiment of the negative pressure precision seed-metering device for wheat. Int J Agric & Biol Eng, 2024; 17(1): 154–162.
[30] Zhao X S, Bai W J, Li J C, Yu H L, Zhao D W, Yin B Z. Study on positive-negative pressure seed metering device for wide-seedling- strip-seeding. Int J Agric & Biol Eng, 2022; 15(6): 124–133.
[31] He X K, Bonds J, Langenakens J. Recent development of unmanned aerial vehicle for plant protection in East Asia. Int J Agric & Biol Eng, 2017; 10(3): 18–30.
[32] Chen X, Chen G L, Wang X D. Optimization design and test of the pore structure of peanut seed metering device. Journal of Zhongkai University of Agricultural Engineering, 2019; 32(1): 28–34. (in Chinese)
[33] Yu J J, Liao Y T, Cong J L, Yang S, Liao Q X. Simulation analysis and match experiment on negative and positive pressures of pneumatic precision metering device for rapeseed. Int J Agric & Biol Eng, 2014; 7(3): 1–12.